Analytical Evaluation of Retarded-Time Potentials of the RWG Bases

Abdulkadir C. Yücel and A. Arif Ergin

Department of Electronics Engineering, Gebze Institute of Technology
Istanbul Cad. No:101, 41400 Gebze, Kocaeli, TURKEY.
acyucel@gyte.edu.tr, aergin@gyte.edu.tr

Abstract

In this study, exact and closed-form expressions for the vector and scalar potentials due to the currents represented by the Rao-Wilton-Glisson (RWG) bases are derived. Calculation of these potentials play a central role in the implementation of the marching-on-in-time (MOT) method for the analysis of surface scattering from structures. To the best knowledge of the authors, these potentials have been numerically calculated in the frequency domain till now, and time-domain applications have inherited similar numerical calculation techniques. In this study, formulae are derived completely in the time domain without any assumptions about the temporal behavior of the RWG basis functions. It is shown that the aforementioned potentials are directly related with the arc segments formed by the triangular patches of the RWG bases and the sphere which is positioned at the observation point and has a radius $R = ct$, where c is the speed of light. Especially, scalar potential is directly proportional to the angles of the total arc segments and the vector potential is a function of the bisector vectors related to these arc segments. A simple algorithm to calculate these quantities is also explained.

1. Introduction

Problems involving electromagnetic scattering from arbitrarily shaped bodies have been solved by numerical procedures. For analyzing scattering problem in the time domain, the Marching-on-in-Time (MOT) method has been widely utilized after 1990s. The most computationally expensive part in the MOT algorithms is the evaluation of the potential integrals related with the space bases functions. One of the widely used space basis functions is the Rao-Wilton-Glisson (RWG) bases [1].

The first step in an MOT method is to discretize the current density on the radiating or scattering body in terms of the RWG basis functions $\mathbf{f}_n(\mathbf{r})$ as

$$\mathbf{J}(\mathbf{r},t) = \sum_n I_n(t)\mathbf{f}_n(\mathbf{r}), \tag{1}$$

where $I_n(t)$ is the time-dependent coefficient corresponding to the n^{th} spatial basis function. With this expansion, the vector and scalar potentials observed at an arbitrary point $\mathbf{r}$ can be expressed respectively as

$$\mathbf{A}(\mathbf{r},t) = \frac{\mu}{4\pi}\int_S \mathbf{J}(\mathbf{r}',t) * \frac{\delta(t-R/c)}{R}dS' = \frac{\mu}{4\pi}\sum_n I_n(t) * \int_S \mathbf{f}_n(\mathbf{r}')\frac{\delta(t-R/c)}{R}dS', \tag{2}$$

$$\phi(\mathbf{r},t) = -\partial_t^{-1}\frac{1}{4\pi\varepsilon}\int_S \nabla'\cdot\mathbf{J}(\mathbf{r}',t) * \frac{\delta(t-R/c)}{R}dS' = -\partial_t^{-1}\frac{1}{4\pi\varepsilon}\sum_n I_n(t) * \int_S \nabla'\cdot\mathbf{f}_n(\mathbf{r}')\frac{\delta(t-R/c)}{R}dS', \tag{3}$$

where $R = |\mathbf{r}-\mathbf{r}'|$ and $*$ denotes temporal convolution. In Eqn. (3), ∂_t^{-1} denotes integration (anti-derivative) with respect to time.

During the implementation of an MOT algorithm, the integrals in Eqns. (2) and (3) are to be evaluated. Currently, these integrations are handled through numerical quadrature. Recently, an approach to find closed-form expressions for these integrals has been proposed [2]. This approach relies on a polynomial approximation of the term $I_n(t) * \delta(t-R/c)$ in Eqns. (2) and (3), through which the result

can be written in terms of time-independent integrals. In this paper, closed-form expressions for the integrals in Eqns. (2) and (3) will be derived. Since these integrals (as formulated above) are independent from the expansion coefficients $I_n(t)$, the results are not based on any a priori assumptions regarding the temporal behavior of the current distributions. To simplify the discussion henceforth, we note that $\mathbf{f}_n(\mathbf{r}) \propto (\mathbf{r}-\mathbf{r}_n)$ over a triangular domain S_n, where $\mathbf{r}_n$ is a given vertex of S_n. Similarly, $\nabla \cdot \mathbf{f}_n(\mathbf{r})$ is a constant over S_n. Using these in Eqns. (2) and (3), and moving the terms independent of $\mathbf{r}'$ out of the integrals yields the critical integrals that are the main subject of this paper. Namely;

$$\mathbf{H}_v(t) = \int_{S_n} (\mathbf{r}'-\mathbf{r}_n)\frac{\delta(t-R/c)}{R}dS', \quad \text{from Eqn. (2)} \quad \text{and} \tag{4}$$

$$H_s(t) = \int_{S_n} \frac{\delta(t-R/c)}{R}dS' \quad \text{from Eqn. (3).} \tag{5}$$

The main aim of this paper can be restated as obtaining closed-form and exact expressions for the integrals (4) and (5).

The rest of the paper is organized as follows. Since the evaluation of a scalar integral is relatively simpler, the evaluation of $H_s(t)$ will be explained in Section 2. In Section 3, where the evaluation of $\mathbf{H}_v(t)$ is discussed, it will become clear that certain geometrical parameters are common to the evaluation of both $\mathbf{H}_v(t)$ and $H_s(t)$. Calculation of these geometrical parameters will be algorithmically explained in Section 4. Verification of the obtained formulas will be accomplished in Section 5 through comparison of the results with those obtained by the inverse Fourier transformation of frequency domain results that employ numerical quadratures.

2. The Scalar Potential Integral

In this section, an exact closed-form expression for $H_s(t)$ will be derived in detail. However, details regarding how the geometrical parameters in the resulting expressions can be obtained will be illuminated later in Section 4. In [3], the frequency-domain counterpart of $H_s(t)$ is recognized as the scalar potential due to a uniform charge distribution over an arbitrary triangular surface S_n. Hence, $H_s(t)$ is the scalar potential due to a temporally impulsive charge distribution over S_n that radiates in a homogeneous, isotropic, and non-dispersive medium. The key to evaluating $H_s(t)$ is realizing that

$$H_s(t) = \frac{1}{t}\int_{S_n} \delta(ct-R)dS'. \tag{6}$$

To arrive at this expression starting from Eq. (5), first, the origin of the coordinate system is shifted so that it coincides with the observation location $\mathbf{r}$. In this shifted coordinate system $R = r'$. Then, the following properties of integration with Dirac functions is employed with $f(r') = 1/r'$:

$$\int f(r')\delta(t-r'/c)dr' = c\int f(r')\delta(ct-r')dr' = c\,f(ct)\int \delta(ct-r')dr'. \tag{7}$$

Finally, Eqn. (6) is obtained by re-shifting the origin back to its original location. It is seen that the integral is related to the arc length of the line formed by the intersection of two surfaces: S_n and the t-parametric surface $ct = R$. This line, labeled l_n, is illustrated in Figure 1(a). Hence, in a sense, the function $H_s(t)$ can be interpreted as the spherical Radon transform of the triangle S_n along the radial direction R. Let us express this insight in mathematical terms.

To evaluate the integral in Eqn. (6), let us define a local (Cartesian) coordinate system (u,v,n), whose origin coincides with $\boldsymbol{\rho}$ (the projection of $\mathbf{r}$ onto the plane of S_n) and unit vectors $\hat{\mathbf{u}}$ and $\hat{\mathbf{v}}$ lie on the plane of S_n as shown in Figure 1(a). Also, let (ζ,ϕ,n) denote the local cylindrical coordinates in

this new system (Figure 1(a)). In this coordinate system, $dS' \equiv \zeta\, d\phi\, d\zeta$. With the definitions of the integration limits illustrated in Figure 1(a), the integral in Eqn. (6) can be written explicitly as

$$H_s(t) = \frac{1}{t} \int_{\zeta_{\min}}^{\zeta_{\max}} \int_{\phi_1(\zeta)}^{\phi_2(\zeta)} \delta(ct - R)\, \zeta\, d\phi\, d\zeta \,. \tag{8}$$

Here, $\zeta_{\min}$ and $\zeta_{\max}$ denote the distance between the point $\boldsymbol{\rho}$ and the nearest and farthest points of S_n to $\boldsymbol{\rho}$, respectively. Since the integrand in Eqn. (8) is independent of ϕ, the inner integration will yield $\alpha_1(\zeta) = \phi_2(\zeta) - \phi_1(\zeta)$, which is the angle spanned by $l_n(t)$. To evaluate the outer integral, a change of variables from ζ to $R = (\zeta^2 + d^2)^{-½}$ can be effected. With these changes and by using Eqn. (7), the explicit expression for $H_s(t)$ can be written as

$$H_s(t) = \frac{1}{t} \int_{R_{\min}}^{R_{\max}} \alpha_1\left(\sqrt{R^2 - d^2}\right) \delta(ct - R)\, R\, dR = \begin{cases} c\,\alpha_1(t) & ; \quad R_{\min} < ct < R_{\max} \\ 0 & ; \quad \text{otherwise} \end{cases}, \tag{9}$$

where $\alpha_1(t)$ is used to succinctly denote $\alpha_1\left(\sqrt{(ct)^2 - d^2}\right)$, since c and d are constants. Eqn. (9) is the exact closed-form expression for the time-dependent scalar potential integral. The only parameter in this expression whose determination is not straightforward is the angle $\alpha_1(t)$. It will be obvious in the next section that during the evaluation of the vector potential integral, vector parameters that depend on this angle will also be needed.

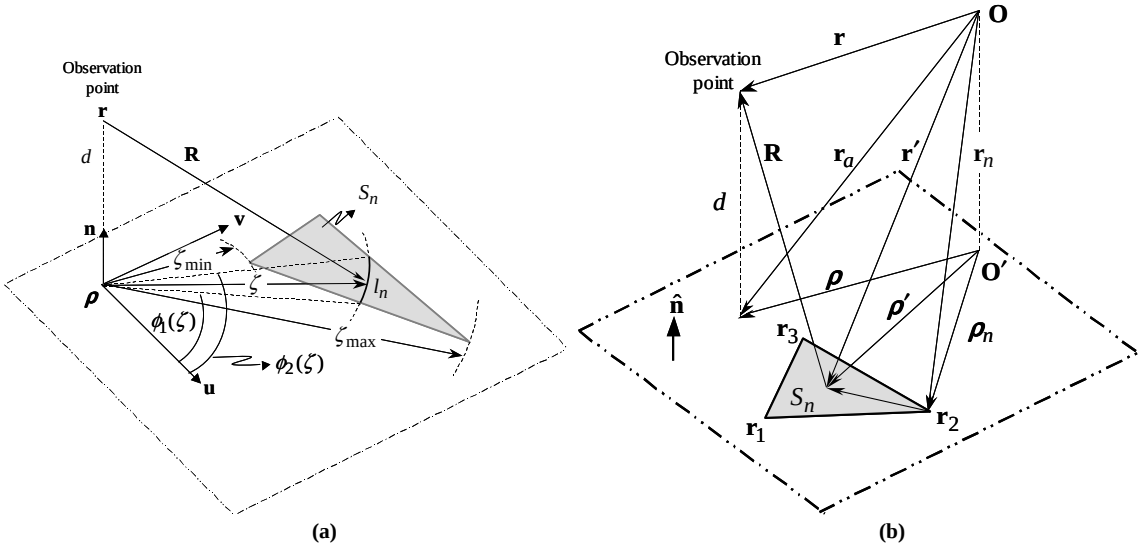

Figure 1 The (u, v, n) and (ζ, ϕ, n) coordinate systems, integration limits (a), and the definitions of relevant vectors (b) .

3. The Vector Potential Integral

In this section, an exact closed-form expression for $\mathbf{H}_v(t)$ given in Eqn. (4) will be derived in detail. In [3], the frequency-domain counterpart of $\mathbf{H}_v(t)$ is recognized as the vector potential due to a vector-valued basis function which is proportional to the vector $(\mathbf{r}' - \mathbf{r}_n)$, where $\mathbf{r}_n$ is the position vector of a vertex of S_n (see Fig. 1(b)) and it is assumed that $\mathbf{r}' \in S_n$. Note that in [3], the vector $(\boldsymbol{\rho}' - \boldsymbol{\rho}_n)$ is used instead of $(\mathbf{r}' - \mathbf{r}_n)$ which are seen to be equal in Fig. 1(b). Henceforth, $(\boldsymbol{\rho}' - \boldsymbol{\rho}_n)$ will be used.

The strategy used to evaluate $\mathbf{H}_v(t)$ is merely an extension of the procedure discussed in the previous section. However, first, $\mathbf{H}_v(t)$ must be split into two terms in order to conveniently apply this procedure. The splitting is effected by using $(\mathbf{r}'-\mathbf{r}_n) = (\boldsymbol{\rho}'-\boldsymbol{\rho}_n) = (\boldsymbol{\rho}-\boldsymbol{\rho}_n)+(\boldsymbol{\rho}'-\boldsymbol{\rho})$ in Eqn. (4), yielding

$$\mathbf{H}_v(t) = (\boldsymbol{\rho}-\boldsymbol{\rho}_n)\underbrace{\int_{S_n}\frac{\delta(t-R/c)}{R}dS'}_{H_s(t)} + \underbrace{\int_{S_n}(\boldsymbol{\rho}'-\boldsymbol{\rho})\frac{\delta(t-R/c)}{R}dS'}_{\mathbf{H}_2(t)}. \tag{10}$$

The first term on the right hand side is recognized as a constant vector times the $H_s(t)$ integral that appears in the scalar potential evaluation of the previous section. To evaluate $\mathbf{H}_2(t)$, let us again use the local cylindrical coordinates (ζ,ϕ,n). Then, in this new system, $\mathbf{H}_2(t)$ can be expressed as

$$\begin{aligned}\mathbf{H}_2(t) &= \int_{S_n}(\boldsymbol{\rho}'-\boldsymbol{\rho})\frac{\delta(t-R/c)}{R}dS' \\ &= \int_{\zeta_{\min}}^{\zeta_{\max}}\int_{\phi_1(\zeta)}^{\phi_2(\zeta)}(\zeta\cos\phi\,\hat{\mathbf{u}}+\zeta\sin\phi\,\hat{\mathbf{v}})\frac{\delta(t-R/c)}{R}\zeta\,d\phi d\zeta \\ &= \frac{1}{t}\int_{\zeta_{\min}}^{\zeta_{\max}}\int_{\phi_1(\zeta)}^{\phi_2(\zeta)}(\cos\phi\,\hat{\mathbf{u}}+\sin\phi\,\hat{\mathbf{v}})\,\delta(ct-R)\,\zeta^2\,d\phi d\zeta,\end{aligned} \tag{11}$$

where Eqn. (7) has been used again to obtain the last expression. Evaluating the ϕ integral first, and then the ζ integral with a change of variables to R, again, produces the final result as follows:

$$\begin{aligned}\mathbf{H}_2(t) &= \frac{1}{t}\int_{\zeta_{\min}}^{\zeta_{\max}}\sin\left(\tfrac{1}{2}\alpha_1(\zeta)\right)\underbrace{\left[\hat{\mathbf{u}}\cos\left(\frac{\phi_1(\zeta)+\phi_2(\zeta)}{2}\right)+\hat{\mathbf{v}}\sin\left(\frac{\phi_1(\zeta)+\phi_2(\zeta)}{2}\right)\right]}_{\hat{\mathbf{e}}_1(\zeta)}\delta(ct-R)\,\zeta^2\,d\zeta \\ &= \frac{1}{t}\int_{R_{\min}}^{R_{\max}}\sin\left(\tfrac{1}{2}\alpha_1(\zeta)\right)\hat{\mathbf{e}}_1(\zeta)\,\delta(ct-R)\,R\sqrt{R^2-d^2}\,dR \\ &= c\sqrt{(ct)^2-d^2}\sin\left(\tfrac{1}{2}\alpha_1(t)\right)\hat{\mathbf{e}}_1(t)\quad;\quad R_{\min}<ct<R_{\max}.\end{aligned} \tag{12}$$

In the final expression, the dependence of α_1 and $\hat{\mathbf{e}}_1$ on t are again expressed in a concise form. Note also that $\hat{\mathbf{e}}_1(t)$ is nothing but the unit vector along the bisector of the angle $\alpha_1(t)$.

4. Obtaining Geometrical Quantities

As mentioned above, determination of the angle $\alpha_1(t)$ and the unit bisector vector $\hat{\mathbf{e}}_1(t)$ is crucial in the evaluation of both the scalar and vector potential integrals. Here, a simple methodology is derived for obtaining these quantities. However, before proceeding further, it should be pointed out that the integration limits in Eqs. (8) and (11) are written somewhat naively to illustrate the concept of derivation. Only for certain values of ζ, the collection of points in S_n that are a distance ζ away from the origin will form a single arc that lies in the range $\phi\in(\phi_1,\phi_2)$. In general, a given value of $\zeta(t)$ will yield $L\le 3$ arcs in S_n. These arcs are formed by the intersection of the triangle S_n with a sphere of radius $R=ct$ (or equivalently, with the circle whose center is $\boldsymbol{\rho}$ and radius is $\zeta(t)=\sqrt{(ct)^2-d^2}$). In this general case, the $\alpha_1(t)$ in Eqn. (9) should be replaced with

$$\alpha(t)=\sum_{i=1}^{L}\alpha_i(t) \tag{13}$$

and the $\sin\left(0.5\alpha_1(t)\right)\hat{\mathbf{e}}_1(t)$ term in Eqn. (12) with

$$\hat{\mathbf{e}}_1(t) = \sum_{i=1}^{L} \sin\left(0.5\alpha_1(t)\right)\hat{\mathbf{e}}_1(t), \tag{14}$$

where the definitions of $\alpha_i(t)$ and $\hat{\mathbf{e}}_i(t)$ are related to the i^{th} arc in S_n. To determine these quantities, first, the intersection of the $\boldsymbol{\rho}$-centered circle with the line segments that bound the triangle S_n must be found. As a result of this step, a group of intersection points $\{\mathbf{c}_k; k \le 6\}$ will be obtained. Then, these intersection points should be grouped in pairs, each of which defines an arc segment within S_n. Finally, the quantities in Eqns. (13) and (14) can be calculated using the $\alpha_i(t)$ and $\hat{\mathbf{e}}_i(t)$ due to each arc segment.

There exist cases when the circle, whose center is at $\boldsymbol{\rho}$ and radius is $\zeta(t)$, does not intersect with any edges of the triangle S_n. In this case, if $\boldsymbol{\rho}$ is located outside of S_n, both $\alpha(t)$ and $\mathbf{e}(t)$ are zero. This case corresponds to the time intervals for which the fields of the current distribution over S_n have either not arrived at the observer location or have already passed it. The latter situation also applies to the case when $\boldsymbol{\rho}$ is located within S_n and $\zeta(t)$ is longer than the distance between $\boldsymbol{\rho}$ and the furthest vertex to this point. Another possibility is that $\boldsymbol{\rho}$ is located within S_n and $\zeta(t)$ is shorter than the distance between $\boldsymbol{\rho}$ and the nearest edge to $\boldsymbol{\rho}$. Here, the whole circle coincides with the interior of S_n and for this reason $\alpha(t) = 2\pi$. Due to the $\sin(0.5\alpha(t))$ term in $\mathbf{e}(t)$, it turns out that $\mathbf{e}(t) = 0$ for this case, too. The last case is quite interesting since it points to the fact that actually there arises no singularity in the scalar and vector potentials as the observation point approaches to the surface which carries the current density.

4. Numerical Results

In this section, the validity of the results in Eqns. (9) and (12) (supplemented with Eqns. (13) and (14)) will be demonstrated through comparison with the results that are first obtained in the frequency domain and then inverse Fourier transformed to time domain. The frequency domain results are calculated by the methods presented in [3].

For many different types of triangles and arbitrarily selected observation points, $H_s(t)$ and $\mathbf{H}_v(t)$ have been evaluated by both time-domain formulation given in this paper (labeled TD in the figures) and by the frequency-domain evaluations (labeled FD in the figures). It is seen that the agreement between the results obtained through the two formulations are gratifying. Nevertheless in here, results that show the salient features of the conducted experiments are presented by using the half RWG basis triangle whose vertex coordinates are $\mathbf{r}_1 = (10,0,1)$, $\mathbf{r}_2 = (15,-5,1)$ and $\mathbf{r}_3 = (15,5,1)$. The current represented on this triangle is assumed to be directed away from $\mathbf{r}_n = \mathbf{r}_1$. In the first example, the observation point $\mathbf{r}$ is positioned at $(5,0,1)$, which lies on the symmetry axis of the triangle. In this case, the circle (with radius $\zeta(t)$) firstly intersects the triangle at vertex $\mathbf{r}_1$ at time $t = 16.7$ ns. Until the circle intersects the edge opposite to $\mathbf{r}_1$ at time $t = 33.3$ ns, there will be a single arc that defines $\alpha(t)$ and $\mathbf{e}(t)$. After this time, there will be two arcs and $\alpha(t)$ will decrease rapidly. These expectations are clearly met as seen in Fig. 2(a) for $H_s(t)$ and $\mathbf{H}_v(t)$.

In the second example, $\mathbf{r}$ is located at point $(11,-6,1)$ to demonstrate the robustness of the developed algorithm under different arc formations at different time intervals. The circle first intersects the triangle at a point over the edge between $\mathbf{r}_1$ and $\mathbf{r}_2$ at time $t = 11.7$ ns. After this time point, the arc segments that contribute to the calculation of $\alpha(t)$ and $\mathbf{e}(t)$ show radical differences in three different regimes bounded by the time points 11.7 ns, 13.7 ns, 20.2 ns, and 39 ns. Therefore, this is a particularly challenging case for the algorithm presented in Section 4. However, as seen from Fig. 2(b), the agreement between the time-domain and frequency domain results is excellent.

It was mentioned in Section 4 that when the observation point is on the basis function, no singularities arise. The third example demonstrates this fact with $\mathbf{r} = (13,0,1)$. In Fig. 2(c), in which the scalar potentials are compared, there are inconsistencies in regions of sharp transition. In other regions, the results show good agreement. The inaccuracies are due to Gibbs phenomenon and reveal the insufficiency of using frequency domain integrations to obtain time domain responses.

So far, only examples with special features and few field components have been presented. The last example is designed to demonstrate the robustness of the proposed algorithm under arbitrarily conditions. Hence, a triangle with vertex coordinates $\mathbf{r}_1 = (-5.20, 6.14, 6.03)$, $\mathbf{r}_2 = (-8.61, 5.36, 12.17)$ ve $\mathbf{r}_3 = (-6.11, 13.14, 6.40)$ is employed. The observation point is at $\mathbf{r} = (-9.43, 0.85, 14.40)$. It is again seen in Fig. 2(d) that both $H_s(t)$ and all the components $\mathbf{H}_v(t)$ show perfect agreement with the results obtained in the frequency domain.

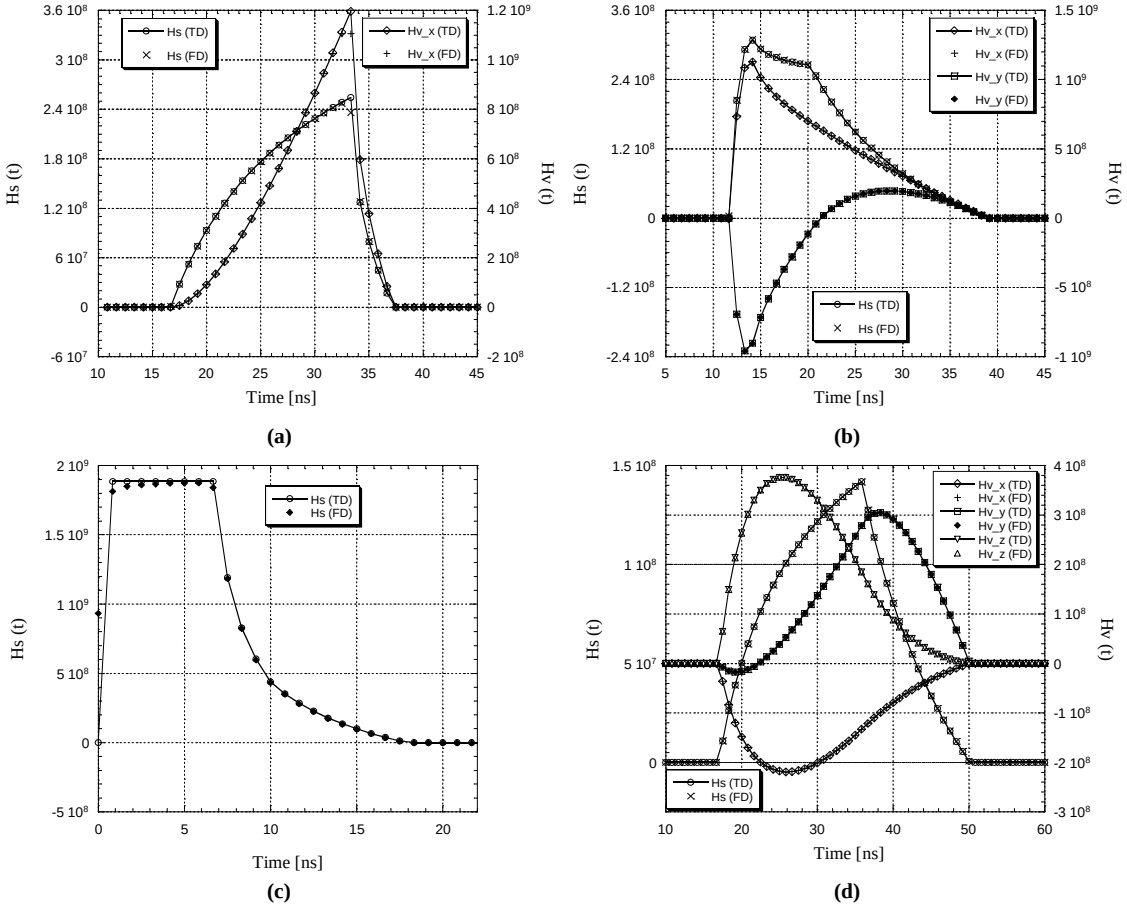

Figure 2 Numerical results for $H_s(t)$ and $\mathbf{H}_v(t)$.

References

[1] S. M. Rao, D. R. Wilton, and A. W. Glisson, "Electromagnetic scattering by surfaces of arbitrary shape," *IEEE Trans. Antennas Propagat*., vol. 30, pp. 408-418, 1982.

[2] M. Lu and E. Michielssen, "Closed form evaluation of time domain fields due to Rao-Wilton-Glisson sources for use in marching-on-in-time based EFIE solvers," presented at Antennas and Propagation Society International Symposium, San Antonio, TX, 2002.

[3] D. R. Wilton, S. M. Rao, A. W. Glisson, D. H. Schaubert, O. M. Al-Bundak, and C. M. Butler, "Potential integrals for uniform and linear source distributions on polygonal and polyhedral domains," *IEEE Trans. Antennas Propagat*., vol. 32, pp. 276-281, 1984.